A Receiver Design for the Superconducting Cavity-Maser Oscillator

R. T. Wang and G. J. Dick
Communications Systems Research Section

A new frequency standard has been demonstrated with the aid of a double phase-locked loop (PLL) receiver. A superconducting cavity-maser oscillator (SCMO) and a hydrogen maser are combined to show the medium-term performance of the hydrogen maser together with improved short-term performance made possible by the SCMO. The receiver, which generates a 100-MHz signal with reduced noise, is phase-locked to (and may be used in place of) the 100-MHz hydrogen-maser output. The maser signal, 2.69xxx-GHz SCMO output, and a 100-MHz quartz-crystal oscillator are optimally combined by the receiver. A measured two-source fractional frequency stability of 2×10^{-14} was obtained for a measuring time of $\tau = 1$ sec, and 1×10^{-15} at $\tau = 1{,}000$ sec. The 1-sec value is approximately 10 times lower than that for hydrogen masers, while the 1,000-sec value is identical to hydrogen-maser performance. The design is based on phase-noise models for the hydrogen maser, the SCMO, and quartz-crystal oscillators for offset frequencies down to 1×10^{-6} Hz.

I. SCMO Operation

The superconducting cavity-maser oscillator (SCMO) is an all-cryogenic, helium-cooled oscillator with superior stability at short measuring times [1–4]. It differs from other superconducting cavity-stabilized oscillator (SCSO) designs [5–7] in its use of a very rigid ($Q \approx 10^9$) sapphire-filled stabilizing cavity and in its all-cryogenic design, with excitation provided by an ultralow-noise cryogenic ruby maser.

The three-cavity oscillator, which consists of a ruby maser, coupling cavity, and a high-Q lead-on-sapphire cavity, has been discussed previously [2]. Oscillation at a frequency of 2.69xxx GHz results from maser amplification in the ruby material, where a population inversion is generated by a 13.1-GHz pump signal. A match between ruby and resonator frequencies is effected by application to the ruby of an approximately 500-gauss bias field. Output power of the oscillator is $> 10^{-9}$ W, more than 1,000 times larger than that of the hydrogen maser, which makes possible $\sqrt{1000} \approx 30$ times higher stability at short measuring times.

The SCMO was recently modified to allow its frequency to be actively adjusted to match that of the hydrogen maser. A coil has been installed on the ruby housing to modify the magnetic bias field by application of a DC current. The coil produces a tuning sensitivity of 7×10^{-12} per mA, with a range of approximately 10^{-10} without significant heating. This range, although only 1/1000 that of a quartz-crystal voltage-controlled oscillator (VCO),

is sufficient to accommodate the typical SCMO drift of 4×10^{-13}/day in long-term operation.

II. Loop Design and Oscillator Noise Models

A double phase-locked loop (PLL) was designed to optimally combine SCMO and hydrogen-maser stabilities. Figure 1 shows a block diagram of that design. Here, one loop locks the phase of a quartz-crystal VCO to the SCMO, while the second loop locks the SCMO/VCO combination to a hydrogen maser through the tuning coil in the SCMO. Design goals are to preserve SCMO short-term stability through the first PLL and optimize the second PLL so that long-term performance of the hydrogen maser is preserved without significantly degrading SCMO performance at $\tau = 1$ sec measuring time. The VCO–SCMO loop characteristics, with a bandwidth of approximately 1,000 Hz, do not significantly impact stability performance when $\tau \geq 1$ sec. However, the SCMO–hydrogen-maser loop does, and so deserves more attention.

While most measurements of the stability of frequency standards are expressed as an Allan deviation $\sigma_y(\tau)$ in the time domain, the results do not directly apply to loop design. This is because the stability (for any measuring time τ) of a source that combines several standards will depend on performance of the contributing standards at *every* τ.

However, the performance of any standard can also be expressed in the frequency domain as a spectral density of phase fluctuations $S_\phi(f)$, and the spectral densities for the various standards at any frequency f simply add, with multiplicative constants determined by loop characteristics at that frequency. Roughly speaking, the unity-gain frequency for the loop will match the crossover frequency between the spectral densities for any two standards being combined.

Although stability measurement data are abundantly available for the DSN hydrogen masers, there existed no measurement of close-in phase noise ($f < 1$ Hz) when the authors undertook their receiver design. Thus, they created a phase-noise model for which the calculated Allan deviation $\sigma_y(\tau)$ matches in detail the results of stability measurements in JPL's frequency standards test facility (FSTF).

Details of this model appear in Table 1. Included for three separate noise components are: noise type, the Fourier frequency window for which the component is dominant, Allan deviation, and phase spectral density. The authors' calculation methodology for generating the Allan deviation corresponding to any phase-noise model is described in the Appendix.

Figure 2 shows a comparison of this model with the results of a very recent calculation of hydrogen-maser close-in phase noise using the same raw data from which Allan deviations were calculated. These data consist of measurements of the time for zero-crossings of a 1-Hz difference frequency using a 100-MHz + 1-Hz reference. The difference between the model and the measured data is within 3 dB for the region from 1×10^{-4} to 1×10^{-1}.

Measurements of the spectral density of phase fluctuations were available for the other two frequency sources. The authors had previously made measurements of the phase noise for the SCMO/SCSO combination for offset frequencies down to 0.01 Hz, and in the absence of any better information, they ascribed half of the measured noise to the SCMO. Other tests of the SCMO with a hydrogen maser as reference indicate a somewhat lower value for offsets below 0.01 Hz. Information for the 100-MHz quartz-crystal oscillator was obtained from the manufacturer.

Figure 3 shows a plot of the phase noises, measured and inferred, for the three oscillators. A smaller contribution due to input noise for the operational amplifier in loop no. 2 is also shown. Crossover frequencies of approximately 0.04 Hz and approximately 1,000 Hz are readily identifiable.

III. Loop-Parameter Optimization

As shown by the dotted line in Fig. 3, calculated performance for the combined source closely approximates the best of the three sources at every frequency. However, deviations from "ideal" performance are significant, as Fig. 4 shows in expanded form, for second-order loops with various loop bandwidths and damping factors. Parameter optimization requires a measure of "goodness" for loop action. It is often the case that performance is optimized for a time period which is much longer than that associated with action of the loop. In this case such an optimization measure can be, for example, rms deviation of the phase error of the following oscillator from the one being followed. In the case at hand, such a single high- or low-frequency measure is not useful because frequencies of concern lie both above and below the crossover frequency.

As shown in Fig. 4, performance deviates significantly from the ideal for frequencies above and below the cross-

over frequency itself. Some applications of the combined source will, for example, emphasize high- over low-frequency performance (or short-term stability for a combined source at the expense of long-term stability). The authors have chosen instead a balanced optimization criterion, which both equalizes and minimizes peak deviations on either side of the crossover.

Successive steps approaching this optimized condition are shown in Fig. 4. A first guess—matching the loop bandwidth to the crossover frequency (0.04 Hz) with a damping factor of $1/\sqrt{2}$—resulted in a large low-frequency peak, substantially worse than any shown in the figure. Equivalent high- and low-frequency performances can be observed in the examples on a diagonal from upper right to lower left. Optimized performance, as shown at the lower left, results primarily from an increased damping factor.

The authors' calculations show continuing small improvement (< 0.2 dB) as the damping factor is further increased. This indicates that on the basis of this criterion alone, an infinite damping factor, corresponding to a first-order loop, would be preferable. However, the larger frequency drift rate of the SCMO, as compared with the hydrogen-maser, necessitates the use of a second-order loop to prevent a slow buildup of phase error, which corresponds to a frequency offset, between the sources. The value of 3 for the damping factor is chosen to give good noise performance and drift immunity combined with relatively rapid loop response.

While spectral densities give a complete representation of performance of the standard, performance in the time domain is a more familiar and widely used measure of performance. Figure 5 shows a calculated Allan deviation for the composite spectral density for the combined sources. It is surprising that stability near the crossover point here is a little better than that of either source, while it closely follows the SCMO and the hydrogen maser at short and longer times, respectively. The slight improvement at the crossover occurs because the Allan deviation for either component standard depends significantly on frequencies both above and below the crossover frequency, and the composite has the advantages of both at the crossover itself.

The calculated combined source shows a stability of 1×10^{-14} at 1 sec and 1×10^{-15} from 1,000 sec onward. The Allan deviation of the combined source follows very closely the best source in the time window of 1–10,000 sec.

IV. Measurements

To confirm the stability of the combined source, a second identical system will be needed. Presently available are hydrogen-masers to test performance at longer measuring times and the SCSO for short-term characterization [5]. Figure 6 shows measurements that demonstrate the short-term stability of the combined source at a test frequency of 100 MHz using the SCSO as a reference. During this test, the poor long-term stability of the SCSO reference substantially degraded the measured values for times $\tau > 30$ sec. However, results at shorter times are as much as 10 times lower than for two hydrogen masers in a similar test. The slight increase for $\tau < 3$ sec has previously been identified as characteristic of the SCSO reference [6], which indicates performance for the authors' combined source of $\sigma_y(\tau) < 1 \times 10^{-14}$ at $\tau = 1$ sec.

Figure 7 shows the Allan deviation of fractional frequency fluctuations for the SCMO locked to a hydrogen maser, using a second hydrogen maser as reference. A special feature is the stability of 6×10^{-14} at 1 sec, a value that is one maser's stability. The transition from "one-maser" noise below $\tau = 30$ sec and "two-maser" noise for longer times causes the slight kink shown in the figure.

V. Conclusions

The authors have designed, built, and demonstrated a receiver that enables the SCMO to operate in conjunction with a hydrogen maser to form a new standard, one which combines their complementary performance over the range of measuring times from 1 to 10,000 sec. Calculated performance for the combined source shows spectral performance $S_\phi(f)$ within 1.4 dB of the best of the two sources over the frequency range 10^{-6} Hz $< f < 10^4$ Hz. Allen deviation is calculated to be within 7 percent of the best of the two sources for measuring times of 1 sec $\leq \tau \leq 10^4$ sec, and somewhat surprisingly, slightly better than either standard at their crossover. Performance for the combined standard was demonstrated in separate experiments using different ultrastable frequency sources to be at least as good as 2×10^{-14} at 1-sec measuring times and 1×10^{-15} at 1,000 sec. Significant aspects of this experiment are a new time window for scientific experiments and a unique demonstration that combines two different types of ultrastable microwave oscillators.

The combined SCMO/hydrogen-maser source underwent a field test at Goldstone Deep Space Communications Complex for 72 days (May–July 1991). The performance was the same as reported above. This exercise was to prepare the SCMO for a gravitational wave detection experiment in connection with Galileo in 1992.

Acknowledgments

Special thanks to the following members of the Communications Research Section: W. A. Diener, for his assistance in ultrastable measurements, R. E. Taylor, for easy access to the capabilities of the Test Facility and assistance with the SCMO field tests, Dr. C. A. Greenhall, for software enhancements meeting the authors' special requirements, T. K. Tucker, for his assistance and support with hydrogen-maser measurements, and Dr. L. Maleki, for his many helpful suggestions.

Table 1. Contributions to the total noise of the DSN hydrogen maser used for loop design

Noise type	Fourier frequency window	Allan deviation	Phase spectral density
Flicker frequency	1×10^{-6} to 4×10^{-4}	1×10^{-15}	$7.5 \times 10^{-15}/f^3$
White frequency	4×10^{-4} to 4.5×10^{-2}	$3 \times 10^{-14}/\tau^{1/2}$	$1.8 \times 10^{-11}/f^2$
Flicker phase	4.5×10^{-2} to 1×10^{-1}	$2 \times 10^{-13}/\tau$	$4 \times 10^{-10}/f$

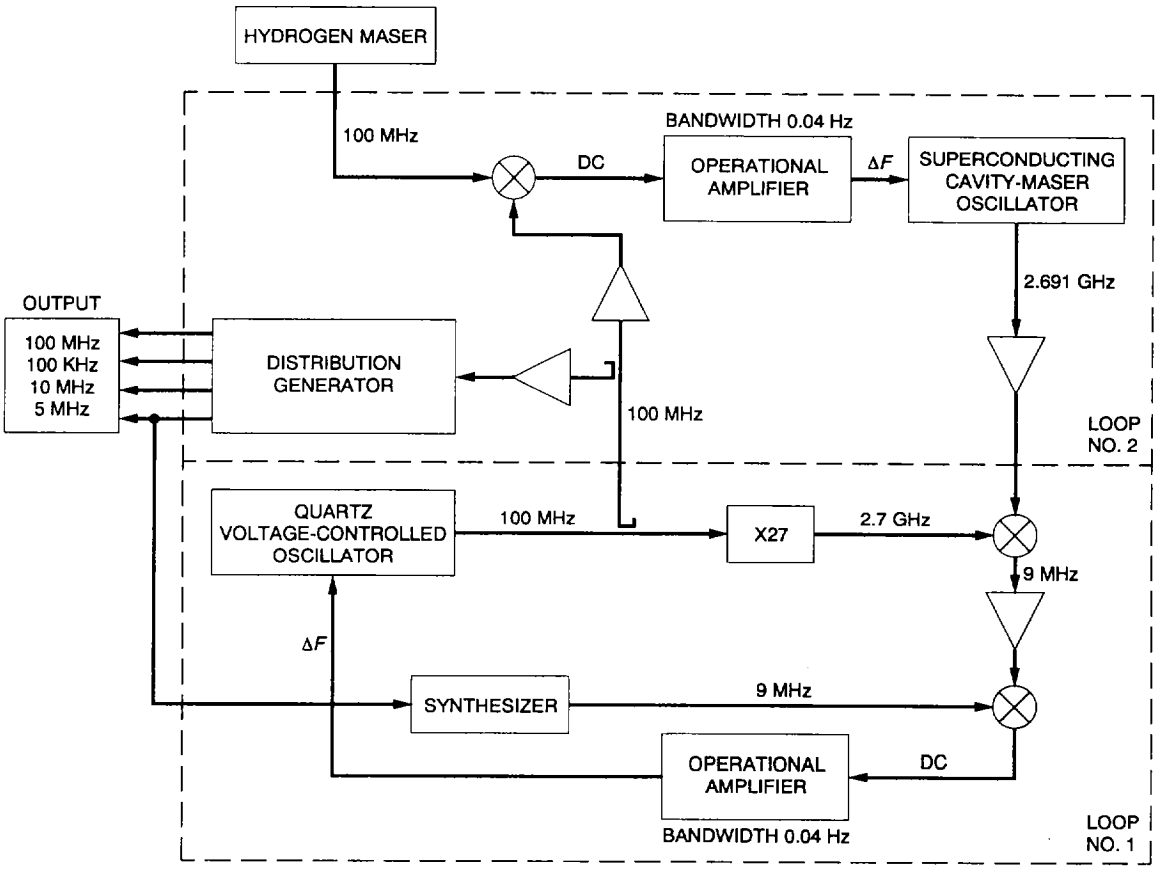

Fig. 1. Schematic of SCMO double-loop receiver at 100 MHz. The two loops are VCO/SCMO and SCMO/hydrogen maser. The required input is the 100-MHz hydrogen-maser signal, and the output has four different frequencies: 100, 10, 5, and 0.1 MHz.

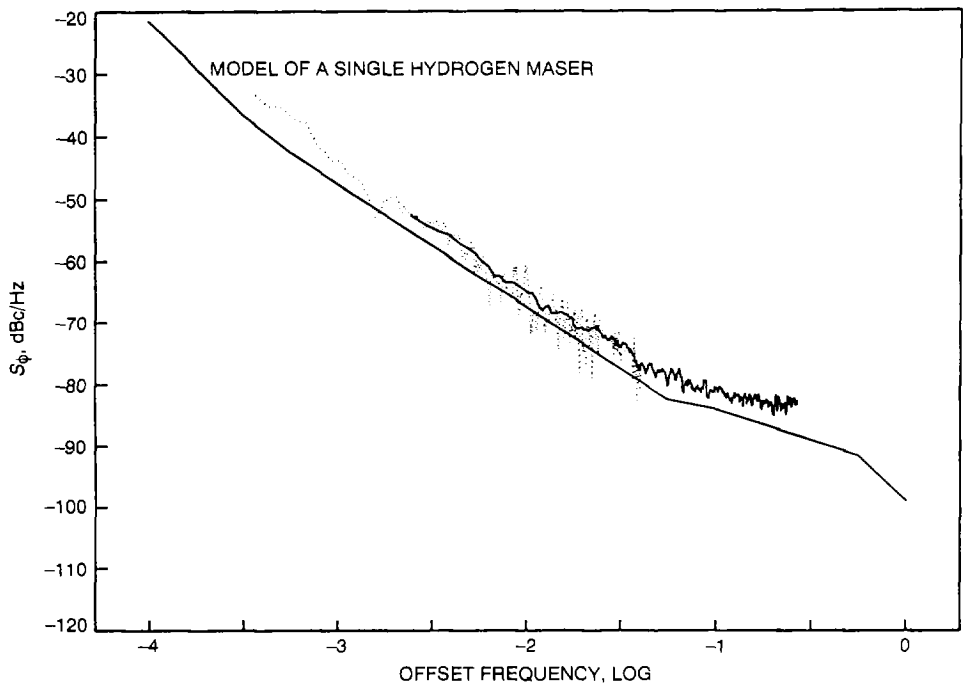

Fig. 2. A close-in phase-noise plot. The solid line shows the model of a single hydrogen maser; two sets of measured pair-data were shown. The difference is within 3 dB for the region from 1×10^{-4} to 1×10^{-1} Hz.

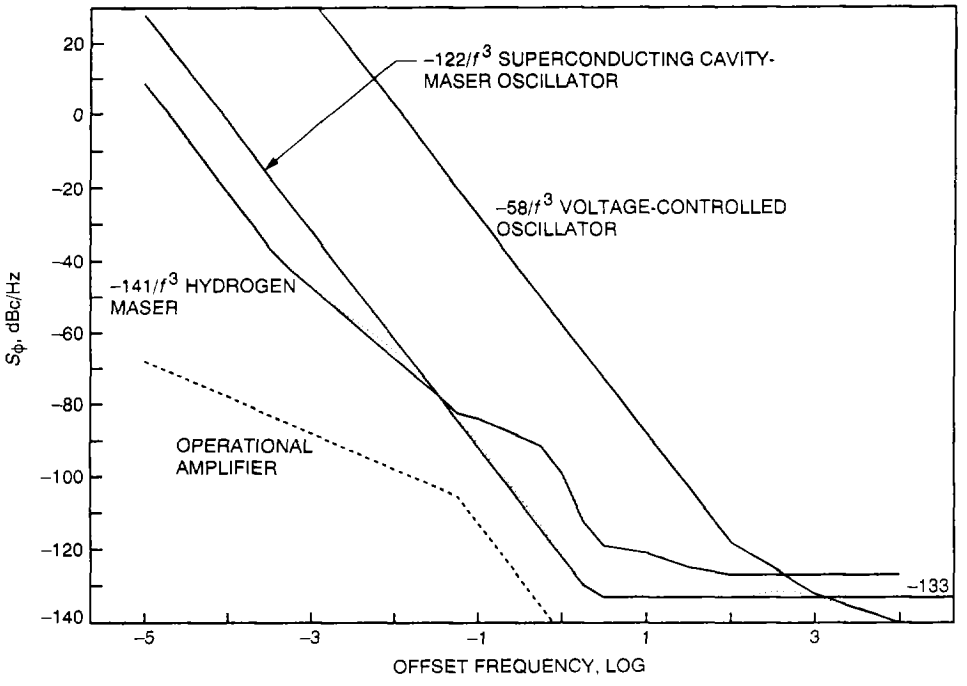

Fig. 3. Phase-noise plot of the three oscillators at 100 MHz. Calculated receiver performance, shown by the dotted line, closely follows the lowest noise of the three oscillators in the Fourier frequency window of 1×10^{-5} to 10^4 Hz. Noise due to the operational amplifier in loop no. 2 is shown to be much lower than oscillator noise contributions.

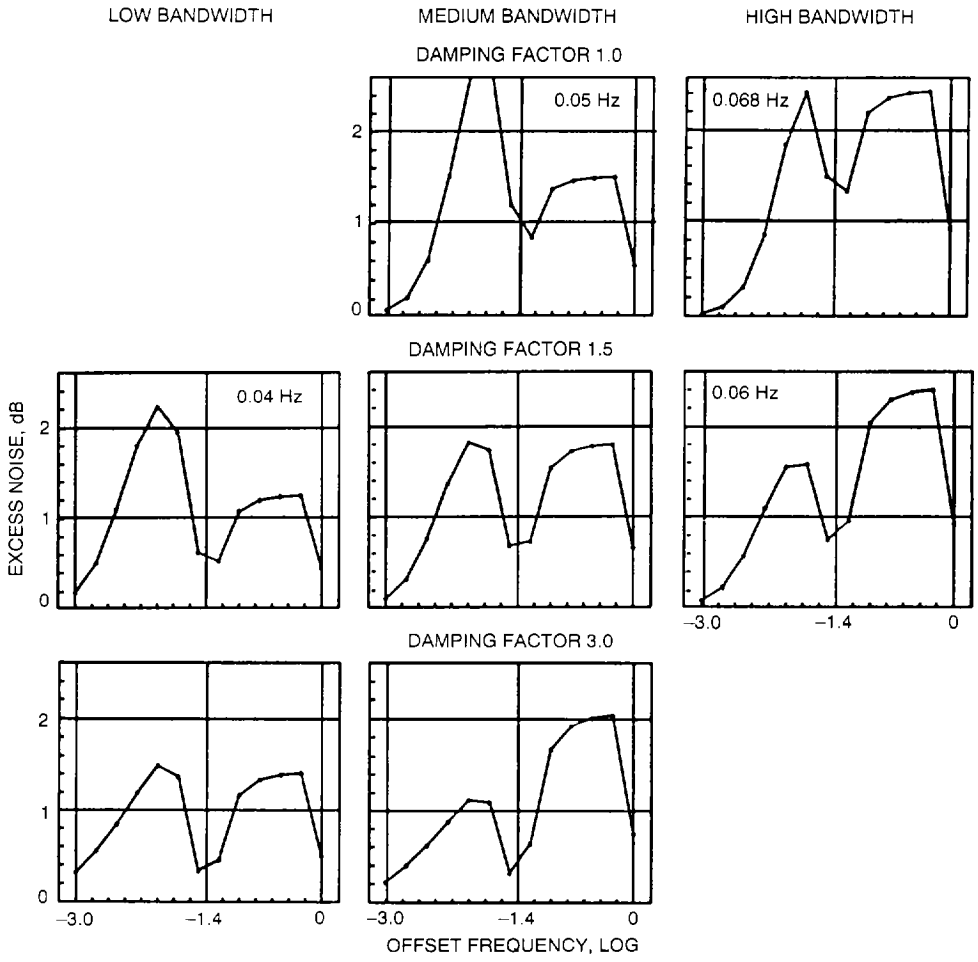

Fig. 4. Optimization of the loop parameters is accomplished by minimizing calculated excess phase noise at the receiver output compared with the best of the constituent oscillators at any given offset frequency. Bandwidths for the various graphs increase from left to right and damping factor increases from top to bottom. Horizontal and vertical scales are identical for each subgraph. Best overall performance, as shown at the lower left, corresponds to a bandwidth of 0.04 Hz (a value equal to the SCMO–hydrogen-maser crossover frequency) and a relatively large damping factor.

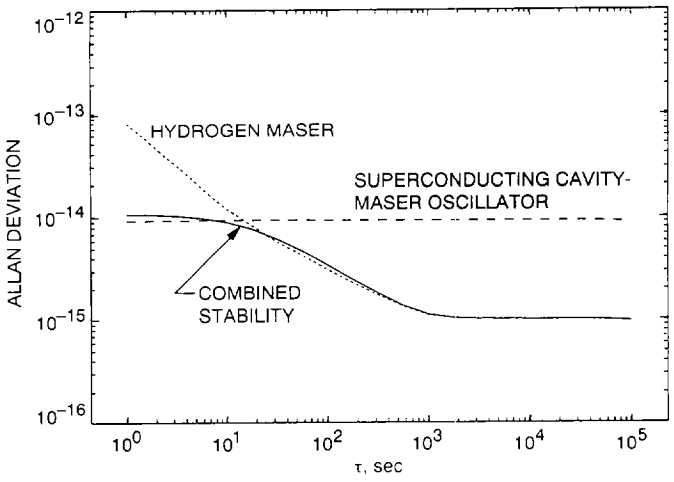

Fig. 5. Allan deviation derived from combined phase noise data (Fig. 3). The expected performance of the combined signal is 1×10^{-14} at 1 sec and 1×10^{-15} at 1,000 sec and beyond.

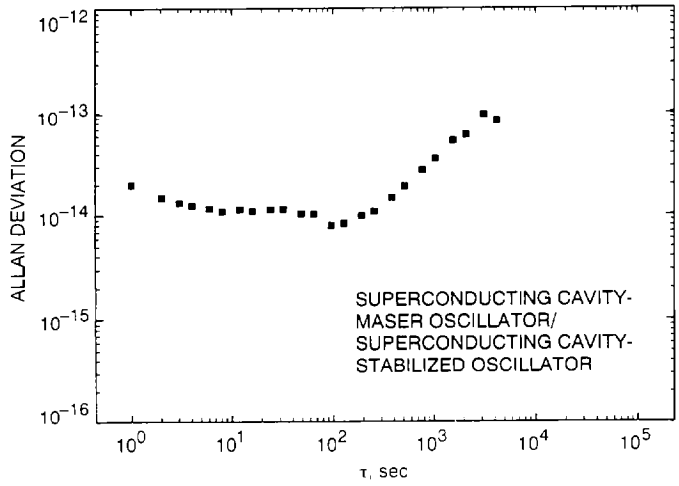

Fig. 6. Two sample Allan deviations of the SCMO tested with SCSO at 100 MHz. The measured frequency stability is 2×10^{-14} at 1 sec. Structure below $\tau = 100$ sec is primarily due to the SCSO reference.

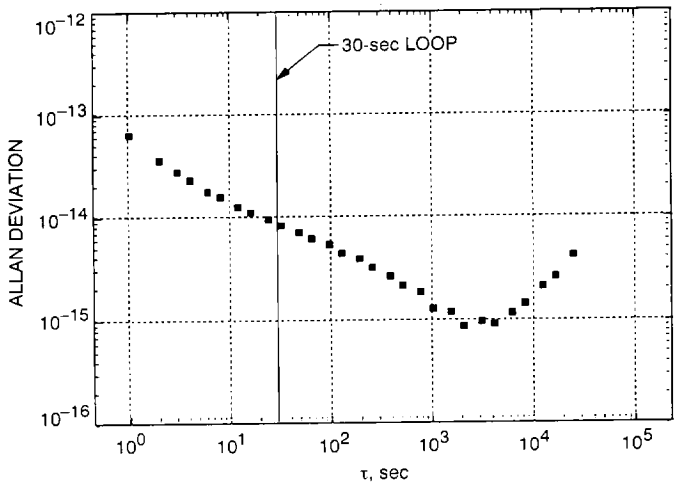

Fig. 7. Two sample Allan deviations of the SCMO locked to one hydrogen maser; the second maser is used as a reference. The vertical line shows the 30-sec loop time constant. The transition from "one-maser" noise below $\tau = 30$ sec and "two-maser" noise for longer times causes the slight kink shown in the figure.

Appendix

Calculation of the Allan Deviation

The Allan deviation of variation of fractional frequency $\sigma_y^2(\tau)$ for any radio frequency (RF) signal can be derived from its spectral density of phase noise $S_\phi(f)$ by using [8]

$$\sigma_y^2(\tau) = \int_0^\infty C(\tau) \times S_\phi(f) \times \sin^4(\pi\tau f) df$$

where

$$C(\tau) = \frac{2}{\pi^2\tau^2\nu_o^2}$$

and ν_0 is the RF frequency. In order to use the numerical integration routines in a popular mathematics program [9] to evaluate this relatively straightforward integral, it is necessary to "condition" the problem in two ways.

First, because significant contributions to the integral are due to frequency components that vary by many orders of magnitude, a change in variable is required, which results in an effectively logarithmic frequency scale. Second, calculation at high frequencies, as compared with $1/\tau$, is hampered by rapid variation in the $\sin^4$ term, which should be replaced by its average value (3/8) as the frequency is raised. It is important for the function that does the replacement to show *very complete* elimination of the average term as the argument $\pi\tau f$ goes to zero so as not to dominate the $(\pi\tau f)^4$ dependence of the $\sin^4$ term.

The change of variable required is straightforward, replacing the frequency f with e^g and the differential df with $e^g dg$. Lower and upper limits to the integration were typically $-6\ln(10)$ and $4\ln(10)$, which corresponds to an integration over frequencies from 10^{-6} Hz to 10^4 Hz.

Elimination of rapid variation is accomplished by replacing

$$\sin^4(\pi\tau f)$$

by

$$Dk\left[\frac{\tau f}{n}\right] \times \left[\sin^4(\pi\tau f) - \frac{3}{8}\right] + \frac{3}{8}$$

where n represents the number of cycles of variation in the $\sin^4$ term that are to be explicitly integrated, and Dk is a decay function defined by

$$Dk(x) = e^{-x\ln(2)}$$

for $x \geq 1$, and

$$Dk(x) = 1 - e^{-\left(\frac{\ln(2)}{x}\right)}$$

for $x \leq 1$. Features of this decay function are extremely rapid approach to 1 for small x, rapid approach to 0 for large x, and continuous first derivative at the crossover point $x = 1$. The authors found $n = 3$ cycles sufficient to reduce fractional errors to less than 10^{-4}.

Taken together, these substitutions allow a difficult integral to be accurately evaluated by means of "canned" integration routines.

References

[1] S. Thakoor, D. M. Strayer, G. J. Dick, and J. E. Mercereau, "A Lead-on-Sapphire Superconducting Cavity of Superior Quality," *J. Appl. Phys.*, vol. 59, pp. 854–858, February 1, 1986.

[2] G. J. Dick and D. M. Strayer, "Development of the Superconducting Cavity Maser as a Stable Frequency Source," *Proceedings of the 38th Annual Frequency Control Symposium*, pp. 435–446, May 29–June 1, 1984.

[3] R. T. Wang, G. J. Dick, and D. M. Strayer, "Operational Parameters for the Superconducting Cavity Maser," *Proceedings of the 20th Annual Precise Time and Time Interval (PTTI) Planning and Applications Meeting*, Vienna, Virginia, pp. 345–354, November 29, 1988.

[4] R. T. Wang and G. J. Dick, "Improved Performance of the Superconducting Cavity Maser at Short Measuring Time," *Proceedings of the Annual Frequency Control Symposium*, Baltimore, Maryland, vol. 44, pp. 89–93, May 23, 1990.

[5] S. R. Stein and J. P. Turneaure,"The Development of The Superconducting Cavity Stabilized Oscillator," *Proceedings of the Annual Frequency Control Symposium*, vol. 27, pp. 414–420, June 12–14, 1973.

[6] S. R. Stein, "Space Application of Superconductivity: Resonators for High Stability Oscillators and Other Applications," *Cryogenics*, vol. 22, pp. 363–371, July 1980.

[7] A. J. Giles, S. K. Jones, D. G. Blair, and M. J. Buckingham, "A High Stability Microwave Oscillator based on a Sapphire Loaded Superconducting Cavity," *Proceedings of the Annual Frequency Control Symposium*, Denver, Colorado, vol. 43, pp. 89–93, May 31–June 2, 1989.

[8] J. Rutman and J. Uebersfeld, "A Model for Flicker Frequency Noise of Oscillators," *Proceedings of the IEEE*, vol. 60, no. 2, pp. 233–235, February 1972.

[9] MathCad 2.0 by MathSoft, Inc., Cambridge, Massachusetts.